Ion-Thruster Propellant Utilization

HAROLD R. KAUFMAN*
NASA Lewis Research Center, Cleveland, Ohio

Maximum propellant utilization in a mercury electron-bombardment thruster is evaluated. The primary-electron region in the ion chamber of a bombardment thruster is analyzed at maximum utilization. Both the analysis and experimental data from a range of ion-chamber configurations show a nearly constant loss rate for un-ionized propellant at maximum utilization over a wide range of total propellant flow rate. The discharge loss level of 1000 ev/ion was used to define maximum utilization. The exact level of this definition has no effect on the qualitative results and little effect on the quantitative results. The results obtained are particularly significant whenever efficient throttled operation is required.

Introduction

THE thrust of a mercury electron-bombardment thruster is provided almost entirely by the ionized portion of the propellant. The un-ionized propellant thus constitutes a loss and should be minimized. A residence-time approach for a neutral in the ion chamber has been tried previously.[1] Although this approach gave the correct qualitative trends for propellant utilization, quantitative agreement was poor. This investigation obtains a better quantitative agreement. An analysis of maximum propellant utilization[2] is the foundation for the theory which herein is compared with experimental data.

The thruster used was originally operated with a 20-cm-diam accelerator system but was masked down to a 10cm system for this investigation. This permitted tests over a wide range of ion chamber configurations including ones with diameters larger than the accelerator system. An electromagnet was used to permit a range of field strengths to be investigated. A strongly divergent magnetic field (with field shaping pole pieces) was employed to be consistent with current designs. Each ion-chamber configuration was operated over a wide range of propellant flow rates from near the lower limit for a sustained discharge to near the upper limit of frequent electrical breakdowns. The thruster was operated both at Colorado State University and at the NASA Lewis Research Center. SI (mks) units are used throughout this paper.

Ion-Chamber Theory

Typical Operation

Electrons are emitted by the ion-chamber cathode, which is maintained 30–40 v negative of the anode. The electrons are constrained by the magnetic field until they collide with propellant atoms. The cyclotron radius for high-velocity emitted electrons is typically 0.1 to 0.5 of the ion-chamber radius. Some of the ions produced by these collisions reach the screen and accelerator grids, where they are accelerated to form the ion beam.

Un-ionized propellant atoms also escape through the accelerator and are the loss of particular interest in this investigation. Thruster efficiency can be defined as the product of utilization and power efficiencies

$$\eta_t = \eta_u \eta_p \tag{1}$$

The thruster efficiency is thus proportional to propellant utilization, and an improvement in propellant utilization can be translated directly into improved thruster performance.

Typical neutral density in the ion chamber is about 10^{18} mercury atoms per m^3. The ions are only about 10% as as dense as the neutrals ($\sim 10^{17}/m^3$), and the electron density equals that of the ions.[3,4] The electron energy distribution corresponds to roughly a 5 ev temperature, although there are significant departures from a Maxwellian distribution that will be discussed later in this paper.

Although the ion density is normally much less than the neutral density in the ion chamber, far more ions than neutrals leave through the accelerator system. This apparent discrepancy is due to the difference in velocities for these two species in the ion chamber. The neutral velocity distribution is essentially Maxwellian and is controlled by the wall temperature. The ions, on the other hand, have a directed velocity toward the boundaries of the ion chamber. This directed velocity is given by Bohm's criterion for a stable sheath.[5]

The path length for the total collision cross section of electrons with neutrals is about 1–3 meters for an electron energy range of 5–40 ev. The large magnitude of this path length compared with ion-chamber size is the reason for using a magnetic field to conserve electrons. The magnetic field is weak enough ($\sim 10^{-3}$ tesla, or ~ 10 gauss), though, that the ion trajectories are essentially unaffected.

The path length for excitation or ionization by 30–40 ev electrons is about 20 m. The electron-electron, coulomb-collision path length (90° collision) for 30–40 ev electrons is about 200 m. Thus, the probability of energy loss due to excitation and ionization for a 30–40 ev electron is much greater than that due to coulomb collisions with background electrons. The population of these energetic electrons, then, is determined by cathode emission rather than a Maxwellian "tail." As a rough approximation perhaps 10% of the electrons are usually found to be energetic "primaries," while the rest make up an essentially Maxwellian distribution. The primary electrons have been found to produce about half the ions in the ion chamber, while the Maxwellian tail produces the rest.[3] This division of ion production is for normal operation and will be a subject of discussion for conditions of maximum utilization.

Residence-Time Approach

The residence-time approach was published in 1965.[1] It assumes a cylindrical ion chamber with an accelerator system covering one end of the cylinder and with uniform conditions throughout the chamber. The utilization expression from the residence time approach is

$$\eta_u = 1 - \exp(-K j_i l) \tag{2}$$

Received August 27, 1971; revision received January 31, 1972. This material is based on a Doctor of Philosophy thesis at Colorado State University.

Index category: Electric and Advanced Space Propulsion.

* Assistant Chief of Electromagnetic Propulsion Division. Associate Fellow AIAA.

where j_i is the ion-beam current density, l is the ion-chamber length, and K is a constant that depends on propellant choice.

For Eq. (2) to correlate the performance of different thrusters, various conditions (such as ion-chamber wall temperature and fraction blockage of the accelerator system) must be nearly the same for different thrusters. In particular, the use of a 20-cm chamber diameter with a 10-cm accelerator system is a sharp departure from the conditions assumed for this equation. In fact, only the 10-cm chamber data presented herein are suitable for comparison with Eq. (2). Inasmuch as these last mentioned data were found to correlate poorly with the parameter $j_i l$, there is no need to modify Eq. (2) for the 20-cm chamber data.

The reason for poor correlation of data from this investigation by the parameter $j_i l$ is believed to reside in the shape of the primary-electron region. The residence-time approach preceded the use of highly divergent magnetic fields, and the primary-electron regions of that period extended the full length of the ion chambers. Thus, a change in ion-chamber length affected the primary-electron region and ion-chamber performance. The primary-electron region in more recent divergent-field designs (as described below) occupies only a fraction of ion-chamber length. Changes in ion-chamber length should therefore not be important for these recent designs unless the chamber becomes very short.

Primary-Electron-Region Approach

This analysis is for high-propellant utilization and is concerned mostly with primary electrons. The primary electrons are concentrated in only a portion of the ion-chamber volume. This portion is essentially the volume enclosed by the accelerator system and magnetic field lines that intersect the anode. The reason for this restriction of primary electrons to a small volume is that the small plasma sheath on the anode does not reflect energetic electrons that can reach it. The existence of a primary electron region is experimentally evident when detailed probe data are available.[3,4] At the high-utilization condition of interest in this analysis, a high fraction of primary electrons is expected. The high fraction is in turn expected to result in primaries causing the bulk of ionizations. These expectations will be supported by probe data. For the thruster investigated herein, the primary-electron region is indicated in Fig. 1. The primary-electron region indicated in Fig. 1 is, of course, somewhat idealized. The finite cyclotron radius of primary electrons leads to a boundary with finite thickness instead of the line thickness of a limiting magnetic field line indicated in the drawing.

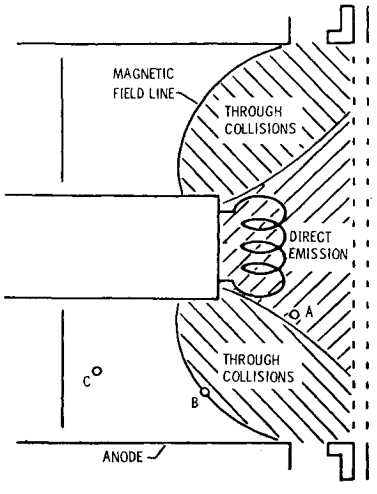

Fig. 1 Primary electron region (shown by cross-hatching) of divergent field thruster used in this investigation. Letters indicate probe locations.

The density of primary electrons increases with discharge current. For a rough approximation, then, the limiting condition of all electrons being primaries can be assumed for maximum utilization. Consider first the total ion production rate $\dot{N}$ from primary electrons. Using mean values for the primary-electron region,

$$\dot{N} = n_p v_p n_o \sigma V_p \tag{3}$$

where n_p and v_p are the primary electron density and velocity, n_o and σ are the neutral density and ionization cross section, and V_p is the volume of the primary-electron region. For the total loss rate of ions from this region

$$\dot{N} = n_i v_i A_p \tag{4}$$

where n_i and v_i are the ion density and velocity toward the outer boundary of the primary-electron region, and A_p is the area of this outer boundary. The ion velocity toward the outer boundary can be estimated from the Bohm criterion for a stable sheath, in which a Maxwellian electron distribution is assumed. The limiting condition of all electrons being primaries would probably depart from a Maxwellian distribution, but the Bohm criterion should still approximate the sheath stability limit. With the mean primary energy used for T_e, the electron temperature, the minimum ion velocity from the Bohm criterion is

$$v_i = v_p(m_e/2m_i)^{1/2} \tag{5}$$

All electrons in the primary-electron region are assumed to be primaries, so that

$$n_p = n_i \tag{6}$$

With the substitution of Eqs. (5) and (6) into (4), and the equating of ion loss and production rates [Eqs. (3) and (4)], one finds

$$n_o = (m_e/2m_i)^{1/2}/\sigma(V_p/A_p) \tag{7}$$

With mercury used for m_i and 5×10^{-20} m^2 used for the ionization cross section σ (40-ev electrons), this becomes

$$n_o = 2.34 \times 10^{16}/(V_p/A_p) \tag{8}$$

A constant neutral density upstream of the accelerator system implies a constant loss of neutrals at maximum propellant utilization regardless of the total mass flow.

The preceding part of this approach [Eqs. (3–8)] was made first.[2] The following extension has been made in an attempt to approximate more closely the effects of a non-Maxwellian electron distribution. This extension unfortunately results in a more complicated expression.

A modified Bohm criterion has been derived by Masek to give the combined effect of monoenergetic primary and Maxwellian electron populations.[3,6] This modified Bohm criterion can be written (at the minimum ion energy) as

$$v_i = v_m[m_e(n_p + n_m)/2m_i n_m]^{1/2} \tag{9}$$

where n_m and n_p are the Maxwellian and primary electron densities, and v_m is the most probable Maxwellian electron velocity. Equation (9) can be rewritten as

$$v_i = v_p[(m_e/2m_i)(T_m/\mathscr{E}_p)(1 + n_p/n_m)]^{1/2} \tag{10}$$

where v_p is the primary electron velocity, and T_m and $\mathscr{E}_p$ are the Maxwellian electron temperature and primary-electron energies—both in ev. The charge neutrality can be expressed in terms of primary and Maxwellian electron populations as

$$n_i = n_p(1 + n_p/n_m)/(n_p/n_m) \tag{11}$$

Substitution of Eqs. (10) and (11) into the loss-rate equation [Eq. (4)] yields

$$\dot{N} = n_p v_p \left(\frac{m_e}{2m_i}\frac{T_m}{\mathscr{E}_p}\right)^{1/2} \frac{(1 + n_p/n_m)^{3/2}}{n_p/n_m} A_p \tag{12}$$

Equation (3) can be used again for the production-rate equation. Equating the loss and production rates

$$n_o = \frac{(m_e/2m_i)^{1/2}}{\sigma(V_p/A_p)} \left(\frac{T_m}{\mathscr{E}_p}\right)^{1/2} \frac{(1 + n_p/n_m)^{3/2}}{n_p/n_m} \tag{13}$$

The mass of a mercury ion can be assumed for m_i, and 5×10^{-20} m^2 used for σ. A value of 5 ev is reasonable for T_m, while ~40 ev would be expected for $\mathscr{E}_p$ in a 40 volt discharge (used throughout this investigation). Equation (13) can then be written as

$$n_o = \frac{0.827 \times 10^{16}}{V_p/A_p} \frac{(1 + n_p/n_m)^{3/2}}{n_p/n_m} \tag{14}$$

The neutral density of Eq. (14) decreases rapidly with increasing n_p/n_m up to about 0.4, and then decreases slowly with further increases in n_p/n_m. The neutral density at an n_p/n_m of 1.0 is in exact agreement with the value predicted by the simpler Eq. (8).

Use of the Bohm Criterion

The original relationship given for the Bohm criterion of sheath stability was[5]

$$v_i \geq (q_i T_e/m_i)^{1/2} \tag{15}$$

That is, the directed velocity of ions toward a collisionless sheath must be equal to, or greater than, a critical value. In making ion-flux calculations for a sheath, however, it is customary to assume a simple equality. The best justification for such an assumption is that it gives results in agreement with experiment.[3,6] Another assumption in the preceding analysis is the use of the Bohm criterion at the upstream boundary of the primary-electron region. This boundary is not a sheath in the ordinary sense. It is, instead, a boundary that separates the primary-electron region with its high ion production rate from the rest of the ion chamber with a much lower ion production rate. This assumed difference in ion production rate is supported by Langmuir probe data. To show the effect of localizing the ion production region, consider Fig. 2. In Fig. 2a the ion production extends throughout the region between two walls, and shows the customary gradual transition from plasma to sheath. In Fig. 2b the ion production has been localized to a central portion of this region. The solution shown in Fig. 2b has been obtained analytically.[7] The ions where found in this analysis to have close to the critical velocity of $(q_i T_e/m_i)^{1/2}$ throughout the two regions of nearly uniform potential shown in Fig. 2b. From Fig. 2b, then, one would expect the Bohm criterion to apply to the entire boundary of the primary-electron region.

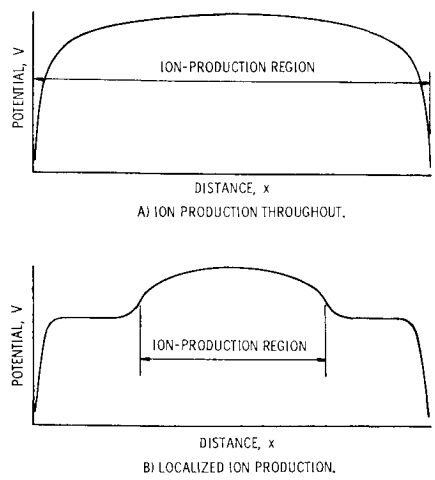

Fig. 2 Form of potential solutions for low-density plasma.

Apparatus

The mercury propellant thruster used is shown in Fig. 3. The magnetic field is determined by a ring shaped, soft-iron pole piece near the accelerator and a cylindrical soft-iron pole piece near the cathode. These pole pieces are connected by four soft-iron paths on which the field windings are mounted. The cylindrical pole piece has about the same cross section as the total of the four paths and also has a field winding for most of its length. Experimental data were taken at various magnetic field currents, but most of the data were obtained at a current of 1 amp. At this current the typical magnetic field in the ion chamber (assumed to be midway between probes A and B in Fig. 1) was about 3×10^{-3} tesla (30 gauss). This field was somewhat nonlinear with current, rising to about 5×10^{-3} tesla for a current of 2 amp.

A 71% open area screen was used to reduce ion recombination on the screen. A tungsten wire cathode was used to avoid both: 1) the uncertainty in propellant utilization that can occur when an oxide cathode is inadvertently overheated, and 2) the effect of localized propellant concentration associated with a hollow cathode.

Ion-chamber probes were made using tantalum wire inside aluminum-oxide tubes. The locations of the probes are shown in Fig. 1. Quartz tubes were used for one set of probe data in an attempt to extend the range of the probe data to higher propellant mass flows by reducing outgassing. Probe location selections were made based on published probe surveys.[6,8] Probe A intersected a magnetic field line near the edge of the cathode and was thought to be representative of the primary-electron region. Probe B intersected a magnetic field line at the boundary of the primary-electron region, while probe C was well removed from that region.

The thruster was operated in vacuum chambers at Colorado State University and at the NASA Lewis Research Center. Pressures in the 10^{-6} torr range were obtained in both facilities.

Procedure

All steady-state operation was at an anode potential of +3000 v and an accelerator grid potential of −1500 v. The total acceleration potential difference of 4500 v was sufficient to handle ion-beam currents of at least 150 ma without any substantial rise in impingement.

The discharge chamber was operated at a potential difference of 40 v for all data presented herein. A range of cathode emissions was obtained for each of several mass flow rates. The cathode emission was limited on the high end of the range by an extinguished discharge, reaching the space-charge emission limit of the cathode, or simply approaching the heater power limit of the cathode. Propellant flows were limited on the low end by inability to sustain a discharge at 40 v and at

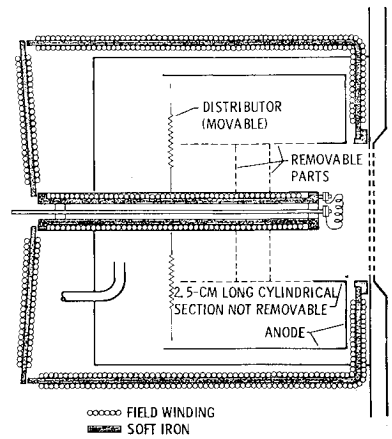

Fig. 3 Thruster with adjustable ion chamber.

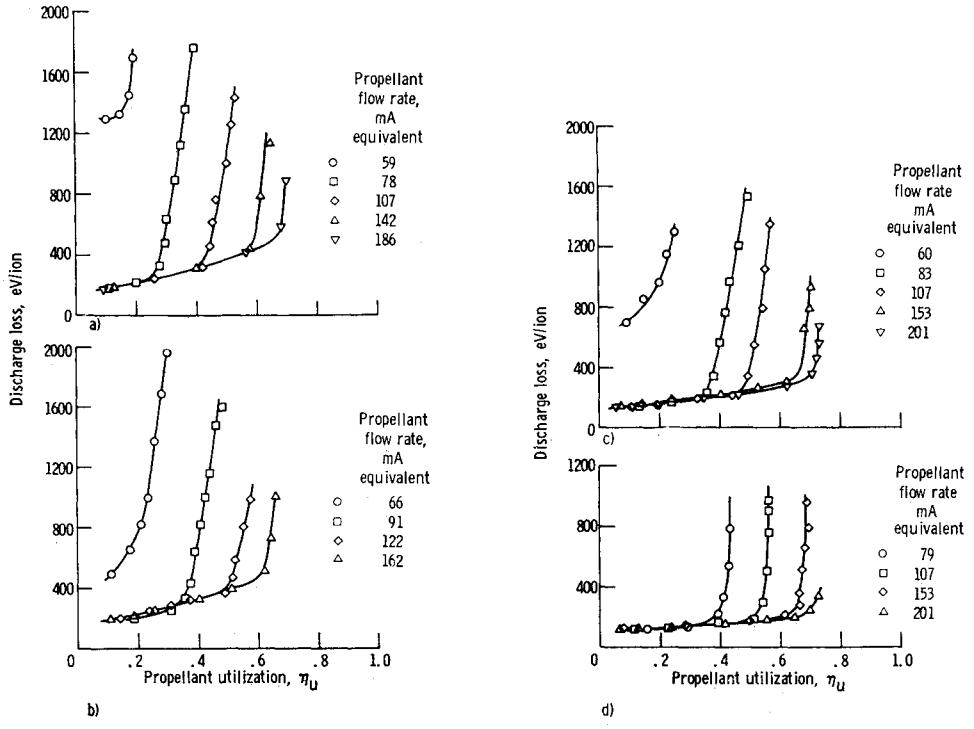

Fig. 4 Ion chamber performance. a) Forward feed, 1 amp magnet, 10 cm diam, 7.2 cm length. b) Forward feed, 1 amp magnet, 10 cm diam, 10.8 cm length. c) Reverse feed, 1 amp magnet, 10 cm diam, 7.2 cm length. d) Reverse feed, 2 amp magnet, 10 cm diam, 7.2 cm length.

the high end by repeated electrical breakdowns between the screen and accelerator grids.

Ion-chamber configurations with three different lengths (7.2, 10.8, and 14.4 cm) were used with a 10-cm diam and two different lengths (9.4 and 14.4 cm) were used with the larger 20-cm diam. These configurations provided a range of about 4 : 1 for ion chamber wall area, and about 8 : 1 for volume. The propellant introduction to the ion chamber was controlled by baffles of polyimide sheet. Most of the data were obtained in the usual mode of straight-through flow from one end of the ion chamber to the accelerator on the other end. This mode is called "forward feed." For comparison, one configuration was operated with "reverse feed," where the propellant was introduced through the gap between the ring shaped pole piece and the anode.

Most of the data were obtained at a magnetic field current of 1 amp, which provided a compromise between good performance at high-mass flow and ability to operate at low-mass flow. Some data were also obtained at higher fields. The theory of plasma probes and their use in ion thrusters has been adequately described in literature,[9,10] and will not be repeated here.

Results and Discussion

Ion Chamber Performance

Typical ion-chamber performance data are shown in Fig. 4. The shapes of the performance curves shown in Fig. 4 (as well as the shapes of similar curves not included in that figure) are typical of electron bombardment thrusters. Each curve has a relatively flat portion below the "knee." The location of the knee and the near vertical portion above the knee depend on propellant flow rate. Comparisons of performance for the near vertical portions of the curves will be adequately covered by subsequent parts of this section. Some comparison of the near horizontal portions below the "knee" is also of interest, however, and will be covered here. Data for the five different configurations are plotted in Fig. 5. The neutral flows for these data range from 142 to 166 ma equivalent (the current that would be measured if each propellant atom carried one electronic charge). This small variation has little effect on the performance below the knee, so that performance in this region can be compared directly. The variation between configurations below the knee is only $\pm 15\%$. In addition, there is no clear trend with ion-chamber volume or surface area. One can conclude that variations in ion-chamber configuration outside of the primary-electron region have no large effect on performance below the knee. Comments by Poeschel et al.[4] indicate that knowledgeable workers in the ion-thruster field would expect such a result.

One might expect a discharge-loss sensitivity to changes in the primary-electron region. This expectation is borne out by the lower losses found at higher magnetic field currents. The higher magnetic field decreases the losses, of course, by making it more difficult for the high-velocity primaries to reach the anode. The use of reverse feed gives a small further decrease in losses, presumably through a change towards a slightly more uniform distribution of ion production in the primary-electron region.

Double valued ion-chamber performance data were not found, except for a small region at high utilization with high magnetic field currents. The extended double valued performance data described in an earlier publication[2] were not encountered after an intermittent magnet winding short was fixed.

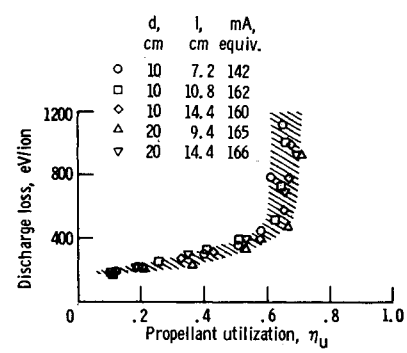

Fig. 5 Comparison of performance for different ion chamber configurations. Forward feed, 1 amp magnet.

Maximum Propellant Utilization

The widest range of operation was obtained at a magnetic field current of 1 amp. For this field current, though, no clear-cut maximum utilization was found (see Fig. 4a–c). Instead, the utilization above the knee increased slowly with increasing losses. As a somewhat arbitrary choice, the utilization at an ion-chamber loss of 1000 ev/ion was used as a maximum. The use of some other high level of loss would have had no effect on the qualitative results presented, and little effect on the quantitative results. Operation at higher magnetic field strength gave close to vertical lines for operation above the knee, so a similar arbitrary choice was not needed. For consistency, though, the same 1000 ev/ion definition was used.

Maximum utilization data are plotted against total propellant mass flow in Fig. 6a for five forward-feed configurations operated at a magnetic field current of 1 amp. The un-ionized propellant mass flow was calculated for the data in Fig. 6a, and plotted in Fig. 6b. This calculation is defined by

$$J_o|_{\text{un-ionizd}} = (1 - \eta_{U,\max})J_o|_{\text{total}} \qquad (16)$$

From Fig. 6b, the maximum utilization data correspond to a constant un-ionized loss rate of 52 ma equivalent, ±8%. This result has considerably less scatter than the previously published maximum utilization data.[2] The reduced scatter is felt to be due to improved experimental techniques, particularly those techniques associated with the long time constants of the thuster used.

The effects of a higher magnetic field and reverse feed of propellant are shown in the maximum utilization data of Fig. 7. Reverse feed gave slightly higher maximum utilization of propellant, but again indicated a near constant loss of un-ionized propellant (about 6–14% lower than Fig. 6). The data for the 2-amp field current (forward feed) agreed more closely with the data shown in Fig. 6, but also showed a slightly lower loss of un-ionized propellant (0–10% lower).

As a general conclusion, then, a highly divergent field thruster shows a near constant loss of un-ionized propellant at maximum utilization. This result can be obtained from either Eq. (8) or Eq. (14) with the proper selection of constants. In agreement with either of these equations of the primary-electron-region approach, the changes outside of the primary-electron region have no significant effect on the loss of un-ionized propellant. Further, even changes that do affect the primary-electron region can have a small effect on this value of propellant loss if the magnetic field shape is constant (which is substantially true of the 1–2 amp range included in Figs. 6 and 7). An interesting point was brought up by a reviewer.

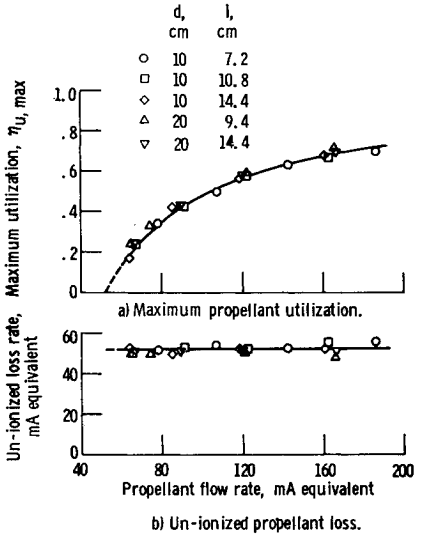

Fig. 6 Correlation of maximum utilization with total propellant flow rate. Forward feed, 1 amp magnet.

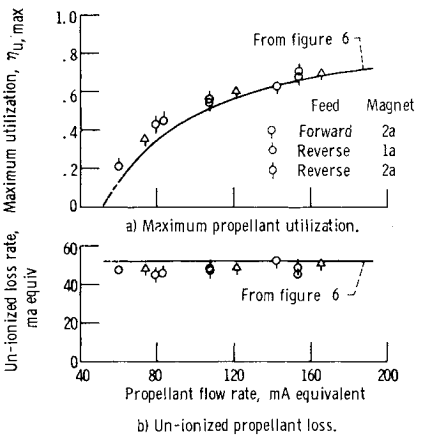

Fig. 7 Effect of feed and magnet current on correlation. Symbols as Fig. 6 except for additions noted.

Equation (8) can be derived as the limiting case of zero utilization for the residence time model [Eq. (2)]. This analytical result would suggest that Eq. (2) should be more valid than Eq. (8), particularly for high utilization. Comparison of the maximum utilization data of Fig. 6 or 7, however, will clearly show that Eq. (2) (with the best fit value of constant) is in poorer agreement with experimental data than either Eq. (8) or (14), and that the lack of agreement is well outside experimental error. This lack of agreement indicates: 1) the derivation of Eq. (8) from the limiting case of zero utilization is accidental with compensating errors in theory, or 2) ion-chamber theory is far from complete. The author is certain the second is true, but not necessarily the first.

Ion-Chamber Probe Data

Thorough Langmuir probe surveys have been made of current divergent field, ion-chamber designs at certain selected operating conditions.[4,6] The objective in obtaining the probe data of this investigation was not to duplicate the published ion-chamber surveys, but to obtain data at a few selected probe locations over a wide range of propellant flow rates and ion-chamber configurations. Probe A (Fig. 7) was selected as a representative sample of the primary-electron region. Probe B was located on the "critical field line" that separates the primary-electron region from the rest of the chamber. Probe C was selected as a representative sample of the ion chamber outside of the primary-electron region.

The ion-chamber probe data were obtained at several emission currents for each of several mass flows. Typical data from probe A are shown in Fig. 8 for one propellant mass flow. The density of Maxwellian electrons first increased with discharge, reached a maximum near the knee of the curve for ion-beam current, then slowly decreased at higher discharge currents. The ratio of primary-to-Maxwellian electron densities increased continuously with discharge current throughout the range investigated. The electron temperature also increased with discharge current, but much less rapidly.

The probe data were cross plotted to determine ion-chamber parameters for the 1000 ev/ion condition defined as maximum propellant utilization. For the data in Fig. 8 the value of 1000 ev/ion is reached at a discharge current of about 2.1 amp. These cross-plotted values are presented in Fig. 9. The scatter in the data of Fig. 9 is to a large extent a measure of the uncertainties involved in obtaining and analyzing ion-chamber probe data. The over-all uncertainty was estimated by Strickfaden and Geiler[9] as being about 30%, with most of the error attributed to the assumption of monoenergetic primary-electron contribution. Frequent replacement of probes was necessary due to cathode sputtering and no doubt added to the total scatter. The cathode sputtering also limited the maximum neutral flow rates at which probe data were obtained.

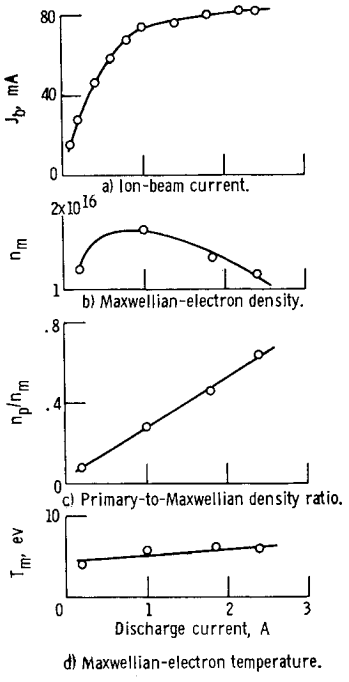

Fig. 8 Typical variation of performance and probe data with discharge (anode) current. Probe A, 131 ma equivalent.

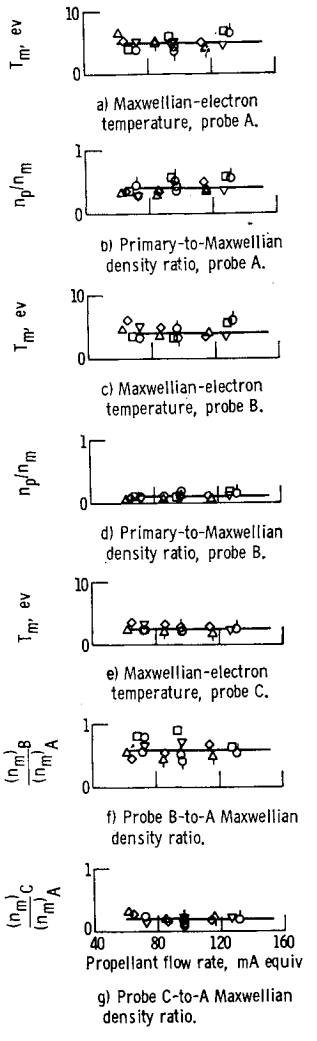

Fig. 9 Ion chamber probe data for maximum utilization. Symbols same as Figs. 6 and 7.

The temperature of the Maxwellian electrons in the primary electron region (probe A, Fig. 9a) averaged about 5 ev, which agrees closely with values obtained previously at lower utilizations.[3] This temperature drops slightly to about 4 ev at the critical field line and is only about 2.5 ev outside the primary-electron region.

The ratio of primary-to-Maxwellian electron densities averages about 0.4 for the primary-electron region (probe A, Fig. 9b). This ratio drops to about 0.1 for the critical field line. Similar data are not shown for the ion chamber outside the primary-electron region (probe C) because the ratio was too low to measure accurately ($\leqq 0.02$). It should be noted that the primary-to-Maxwellian density ratio in the primary-electron region is well above the $\leqq 0.1$ value found previously at more normal operating conditions. This high value is due to the 1000 ev/ion discharge losses used for Fig. 9. One should also note that the electron parameters for this high-discharge loss indicate that most of the ionization will take place in the primary-electron region, as assumed in the analysis. The mean energy of the primary electrons ranged from about 35–40 ev at probe A, 30–35 ev at probe B, and <30 ev at probe C.

The data shown in Fig. 9 show no significant trends with propellant mass flow or ion-chamber surface area. The use of the mean values of 5 ev for Maxwellian-electron temperature T_m and 0.4 for primary-to-Maxwellian density ratio n_p/n_m appears justified for the primary-electron region values of Eq. (14). (T_m and n_p/n_m enter with considerably less than linear effects in Eq. (14), so that the scatter for these parameters shown for probe A in Fig. 9 is not important.) The values of T_m and n_p/n_m, together with a value of 0.011 m for V_p/A_p (which can be obtained from a magnetic field map such as shown in Fig. 1), give a neutral density of $3.11 \times 10^{18}/m^3$.

An unpublished analysis by W. R. Kerslake indicated an effective flow factor of about 0.5 for the open area of a SERT II accelerator grid. The thruster used herein had the same screen and accelerator grid thicknesses and hole diameters, and thus should have the same flow factor. The accelerator open area was 50% of a 10-cm diam beam, so that this factor of 0.5 resulted in an effective sharp edged orifice area of 0.00196 m^2. This effective orifice area, the neutral density of $3.11 \times 10^{18}/m^3$ and an assumed wall temperature of 500° K result in a neutral loss rate of 56 ma equivalent. This value is quite close to the experimentally determined value of 52 ma (Fig. 6). This close agreement is well within the possible error of the analytical model and constitutes an independent check on the analytical model.

Comparison with SERT-II Data

It is of interest to compare the results of this investigation with published data. Probably the most documented thruster of divergent-field design is the one used on the SERT-II flight.[11] The SERT II throttling data[12] were reviewed, and found to show the same nearly constant loss rate for un-ionized propellant that was found in this investigation. The comparison was not possible for the full throttling range above 250 ev/ion. But this value was high enough to be in the knee of the loss curve, and thus be substantially proportional to maximum utilization as defined herein. The un-ionized propellant loss ranged over 45–50 ma equivalent for 250 ev/ion and a total propellant flow range of 2.5 to 1.† The level of un-ionized propellant loss rate predicted from the theory of this investigation, however, was substantially above the observed range of 45–50 ma equivalent. An unusual aspect of SERT II ion-chamber operation (with the accelerator system used for the throttling data[11]) was for formation of several volt ridges in plasma potential near the anode.[4,8] Although the cause of these potential ridges is not clear, their presence probably reduced radial ion losses in their vicinity. If one neglects the boundary area of the primary-electron region near these

† From private communication with Byers, Fig. 6b[12] is incorrect. The utilization at 250 ev/ion and a beam current of 0.20 amp was close to 0.80.

ridges, the calculated neutral loss becomes much closer to the experimental values. Also, the introduction of propellant through the hollow cathode (about $\frac{1}{3}$ of the total propellant flow at SERT-II design conditions) was a departure from the uniform conditions assumed for the theory derivation. Thus, although SERT-II data is in good qualitative agreement with the theory of this investigation, it is apparently possible to obtain special plasma conditions that will affect the quantitative agreement of experimental data with the theory presented here. There is no evidence for reduced radial ion loss in the present investigation, inasmuch as probes A and B had an average potential difference of less than 1 v.

Conclusions

The results of this investigation can be expressed simply: the loss rate of un-ionized propellant at maximum utilization is nearly a constant over a wide range of total propellant flow rate, permitting rapid prediction of total flowrate effects from operation at one total flow rate. These results are particularly significant for throttled operation of a fixed configuration thruster. Because of variations in available power, many missions require operation at less than maximum thrust. To avoid large power losses or propellant losses, such part-thrust operation should be near the knee of the ion-chamber loss curve. This knee will shift substantially in the same manner as maximum propellant utilization. Inasmuch as the un-ionized propellant loss rate will be a larger fraction of total flow rate at part-throttle operation, one can expect the most difficult requirement for utilization to be at the lowest thrust level to be used. Without any configuration changes accompanying thrust reduction, then, a thruster with good part-thrust performance would be expected to have very high utilization at full thrust. Good qualitative agreement of these results was found with published SERT-II throttling data.

References

[1] Kaufman, H. R., "Performance Correlation for Electron-Bombardment Ion Sources," TN D-3041, 1965, NASA.

[2] Kaufman, H. R. and Vahrenkamp, R. P., "Some Performance Characteristics of Divergent-Field Bombardment Thrusters," AIAA Paper 70-1092, Stanford, Calif., 1970.

[3] Masek, T. D., "Plasma Properties and Performance of Mercury Ion Thrusters," TR-32-1483, NASA CR-110731, June 1970, Jet Propulsion Lab., California Inst. of Technology, Pasadena, Calif.

[4] Poeschel, R. L., Ward, J. W., and Knauer, W., "Study and Optimization of 15-cm Kaufman Thruster Discharges," *Journal of Spacecraft and Rockets*, Vol. 7, No. 1, Jan. 1970, pp. 26–30.

[5] Bohm, D., "Minimum Ionic Kinetic Energy for a Stable Sheath," *The Characteristics of Electrical Discharges in Magnetic Fields*, edited by A. Guthrie and R. K. Wakerling, McGraw-Hill, New York, 1949, pp. 77–86.

[6] Masek, T. D., "Plasma Properties and Performance of Mercury Ion Thrusters," *AIAA Journal*, Vol. 9, No. 2, Feb. 1971, pp. 205–212.

[7] Dunn, D. A. and Self, S. A., "Static Theory of Density and Potential Distribution in a Beam-Generated Plasma," *Journal of Applied Physics*, Vol. 35, No. 1, Jan. 1964, pp. 113–122.

[8] Knauer, W., Poeschel, R. L., King, H. J., and Ward, J. W., "Discharge Chamber Studies for Mercury Bombardment Ion Thrusters," NASA CR-72440, Sept. 1968, Hughes Research Labs., Malibu, Calif.

[9] Strickfaden, W. B. and Geiler, K. L., "Probe Measurements of the Discharge in an Operating Electron Bombardment Engine," *AIAA Journal*, Vol. 1, No. 8, Aug. 1963, pp. 1815–1823.

[10] Kerrisk, D. J. and Masek, T. D., "Plasma Nonuniformity and Grid Erosion in an Electron Bombardment Ion Engine," *AIAA Journal*, Vol. 3, No. 6, June 1965, pp. 1060–1066.

[11] Kerslake, W. R., Byers, D. C., and Staggs, J. F., "SERT II: Mission and Experiments," *Journal of Spacecraft and Rockets*, Vol. 7, No. 1, Jan. 1970, pp. 4–6.

[12] Byers, D. C. and Staggs, J. R., "SERT II: Thruster System Ground Testing," *Journal of Spacecraft and Rockets*, Vol. 7, No. 1, Jan. 1970, pp. 7–14.